ISSN 1024-8560, Atmospheric and Oceanic Optics, 2021, Vol. 34, No. 2, pp. 117–127. © Pleiades Publishing, Ltd., 2021.
Russian Text © The Author(s), 2020, published in Optika Atmosfery i Okeana.

ACOUSTOOPTICAL AND RADIOOPTICAL METHODS FOR ENVIRONMENTAL STUDIES

Height of the Region of Intense Turbulent Heat Exchange in a Stably Stratified Boundary Layer of the Atmosphere. Part 2: Relationship with Surface Meteorological Parameters

S. L. Odintsov[a, b, *], V. A. Gladkikh[a], A. P. Kamardin[a], and I. V. Nevzorova[a]

[a] *V.E. Zuev Institute of Atmospheric Optics, Siberian Branch, Russian Academy of Sciences, Tomsk, 634055 Russia*
[b] *National Research Tomsk State University, Tomsk, 634050 Russia*
**e-mail: odintsov@iao.ru*

Received July 14, 2020; revised July 14, 2020; accepted October 6, 2020

Abstract—The second part of the paper is devoted to the analysis of how heights of intense turbulent exchange and their corresponding temperature gradients in the atmospheric boundary layer are interrelated with ground values of the wind velocity and vertical turbulent heat flow. We consider only cases of temperature inversions in winter (January–February 2020). The division of inversions into two types (ground and raised) and four forms is introduced and the statistic for the height of the turbulent exchange region is obtained for them. According to results of the analysis, a conclusion is made that the direct (well-defined) relation between the height of the intense turbulent heat exchange layer and ground values of the wind velocity and turbulent heat flow is absent under conditions of temperature inversions.

Keywords: temperature inversion, atmospheric boundary layer, surface layer, wind speed, sodar, temperature profiler, turbulent heat exchange, sonic anemometer/thermometer

DOI: 10.1134/S1024856021020068

INTRODUCTION

In many works, when simulating the structure of the atmospheric boundary layer (ABL), processes and fields are parameterized using approaches based on the information about ground values of different meteorological parameters. In particular, the ABL height (we denote it as H_{ABL}) is estimated using ground values of the vertical turbulent heat flow, temperature variance, wind velocity or derivatives of it—the friction velocity (dynamic velocity), kinetic energy of turbulence and/or its dissipation rate, and so on (see, e.g., [1–9] and references therein). However, almost all studies emphasize that the technique for the determination of H_{ABL} should be refined in cases of temperature inversions.

By the boundary layer we mean the region with the presence of turbulent flows of heat and momentum without a clear separation of the spatiotemporal structure of these factors. Zones with an intense turbulent heat exchange (we denote the height of such zones as H_m) and an intense transfer of the momentum (H_R) overlap each other. The equality $H_m = H_R$ is by no means always valid for them. It is clear that the condition $H_{\mathrm{ABL}} = \max\{H_m, H_R\}$ must be satisfied. As a rule, the inequality $H_m < H_R$ holds and, for this reason, it is usually assumed that $H_{\mathrm{ABL}} = H_R$. This is corroborated by results of processing the experimental data obtained in the complex investigation of the ABL, e.g., with the use of lidars, radiosondes, and sodars [8–18]. In particular, lidars monitor regions with a high concentrations of aerosol which is redistributed mainly under the influence of wind turbulence. Therefore, lidar methods provide the estimate $H_{\mathrm{ABL}} = H_R$. Results of radiosonde operations are used, e.g., for estimates of height profiles of the Richardson numbers. Their value determines the level above which the wind flow is considered as laminar. Therefore, this technique also yields the estimates $H_{\mathrm{ABL}} = H_R$. Only sodars (meteorological acoustic locators) can at present provide a direct estimate of H_m.

The version in which, based on some known ground values of parameters, one can reconstruct (predict) height–time profiles of ABL characteristics of interest with satisfactory accuracy by means of relationships established between high-altitude and ground data with the use of empirical (or theoretical) investigations would be most optimum for the prediction of the ABL state. It is desirable to have an opportunity to estimate the height $H_{\mathrm{ABL}} = \max\{H_m, H_R\}$. However, in our opinion, the present-day parameterization quality of such relationships for conditions of stable stratification is unsatisfactory.

The general purpose of this work is to study the turbulent heat exchange in the ABL under conditions of

temperature inversions in winter. In the first part of the paper [19], the methodological basis of obtaining the data about the height H_m and about absolute air temperature gradients γ_m corresponding to this height was expounded, and the general statistic of these parameters was presented. The aim of the second part of the paper is the analysis of how the quantities H_m and γ_m are interrelated with the wind velocity V_h and the turbulent heat flow Q_t near the underlying surface, to verify the possibility of using these parameters in estimates (predictions) of H_m and γ_m. Herewith, it is not assumed that $H_{ABL} = H_m$, i.e., one should not identify the height H_m with the height of the ABL. Note that H_m was studied using sodars, e.g., in [8–13].

EQUIPMENT, PLACES, AND MEASUREMENT MODES

The analysis is based on experimental data obtained using temperature–wind complexes operating in January–February 2020 at the Base Experimental Complex (the BEK point, a natural landscape) of the Institute of Atmospheric Optics (IAO) and in the territory of the Akademgorodok microdistrict (on the outskirts of Tomsk, an urbanized territory, the IAO point). The temperature–wind complex included a Volna-4M sodar, an MTP-5 meteorological temperature profiler, and Meteo-2 ultrasonic meteorological stations (UMSs). More detailed information about their technical characteristics and operation regime was presented in [19–23].

We recall that the analysis for the IAO point was carried out only for the period 08:00–21:00 LT when the sodar was incorporated into the complex operated in active mode. The other devices operated around the clock. A total of 505 h of observations were processed at this point; among them, air temperature inversions (ground or raised) were observed for 284 h in the ABL in the range 0–1000 m. At the BEK point, the complex could operate around the clock. The total time available for the analysis at this point was 888 h; of which 611 h were temperature inversions.

TYPES AND FORMS OF TEMPERATURE INVERSIONS

Before turning to the analysis of the relationships of H_m and γ_m with meteorological parameters, we consider in more detail the statistics of types and forms of temperature inversions for January–February 2020. Figure 1 presents model profiles of the absolute air temperature; they correspond to real ones in the period under study. The temperature inversions were divided into two types. Type 1 corresponded to ground inversions (Fig. 1a); type 2, to raised inversions (Fig. 1b). Each of the types, in turn, was divided into four forms numerated in Fig. 1. Hereinafter, the notation (indices) for the inversions is encountered,

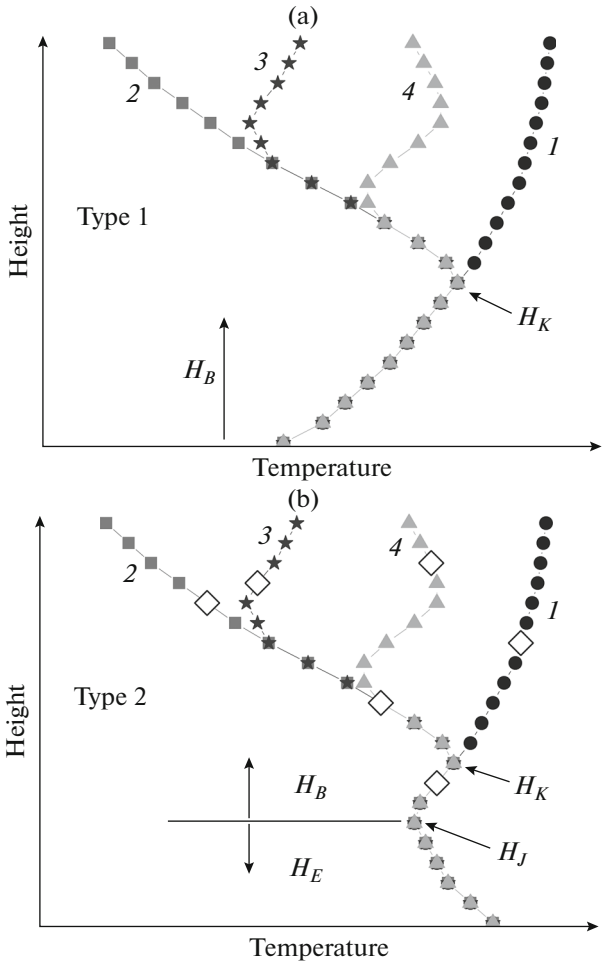

Fig. 1. Model profiles of the absolute air temperature of (a) type 1 (ground inversions) and (b) type 2 (raised inversions); the figures denote different forms of inversion; the open symbols in the plots are examples of the position of the intense turbulent heat exchange layer height H_m on the temperature profiles; other notations are explained in the text.

e.g., in the form 24, which means inversion type 2 in form 4 (plot *4* in Fig. 1b).

The statistics of different types and forms of temperature inversions at the observation points is given in Table 1. It presents total durations (hours, rounded) of different forms of the inversions.

According to the results presented in Table 1, inversions in form 2, i.e., single-layer inversions limited in height (indices 12 and 22) dominated in the layer 0–1 km. In addition, we note that two-layer inversions took place most often in the case of ground inversions (index 14) and rarely occurred in the case of raised inversions (index 24).

Note also that the number of type 1 inversions at the IAO point was significantly less than at the BEK point. This seems to be caused by two factors. The first one is that measurements at the IAO point were car-

ried out only from 08:00 to 21:00, when by the beginning of measurements the processes of ground inversion transformation were already activated under the action of the Sun warming the snow-covered underlying surface. Results for BEK included also nighttime conditions under which the implementation of ground inversions is most probable. The second factor is the influence of man-made heat sources in the territory where the IAO point is situated.

It is natural that one type of inversion is transformed into another in the daily variations of height profiles of air temperature. We have distinguished different forms through which the inversion type passes in this process. A thorough study of such processes is undoubtedly important for refining algorithms for the prediction of the ABL state. At this stage of the work, however, we did not deal with the solution of the abovementioned problem and restricted ourselves only to the analysis of the turbulent heat exchange penetration into temperature inversions. The specificity of the analysis is the consideration of winter conditions when a snow cover is observed on the underlying surface and its heating by solar radiation and the turbulent heat exchange have unique features.

A considerable number of cases where the inequality $\gamma_m \le 0$ was satisfied at the height H_m, i.e., the turbulent heat exchange either did not penetrate into the temperature inversion or completely covered it, were already mentioned in [19]. The first case is related to raised inversions (type 2). In Fig. 1b, this region is below the horizontal line (H_E region). The height of the lower boundary of the inversion layer is marked as H_J. Below, we assume that the equality $H_J = 0$ is valid for type 1 inversions. The upper boundary of the lower inversion layer is denoted in Fig. 1 as H_K (for both inversion types). Let us consider three versions of the position of height H_m on the temperature profile. By version 1 we mean cases where $H_J < H_m < H_K$ ($\gamma_m > 0$), i.e., the turbulent heat exchange penetrates into the temperature inversion but does not reach its upper boundary.

In region H_B which contains the inversion, values $\gamma_m \le 0$ can be negative. This means full overlapping of the lower inversion layer by the turbulent exchange and fulfillment of the inequality $H_m \ge H_K$ (regardless of the type and form of the inversion). We denote this case as version 2.

In region H_E (see Fig. 1b), $H_m \le H_J$ and $\gamma_m \le 0$, i.e., the turbulent exchange does not penetrate into the temperature inversion; this is version 3 of the position of the upper boundary of the region with an intense turbulent exchange.

The duration of different versions of the position of height H_m on temperature profiles at the IAO and BEK points is presented in Table 2. Let us pay attention to the fact that, at both points in the case of ground inversions (type 1), versions 1 and 2 were implemented during approximately the same time. It means that overlapping of ground inversions by the turbulent heat exchange is a common fact.

Table 1. Statistics of temperature inversions—total durations of the implementation (diagnostics according to the layer 0–1 km)

Type	Form				Total
	1	2	3	4	
IAO point (08:00–21:00)					
1	3	35	1	13	52
2	67	156	7	2	232
BEK point (00:00–24:00)					
1	25	121	22	77	245
2	120	218	6	22	366

Table 2. Duration of different versions of the position of the turbulent heat exchange region height H_m in the layer 0–1 km (hours, rounded)

Type/duration of the inversion	Version			
	1	2	1 + 2	3
IAO point (08:00–21:00)				
1/52	26	26	52	–
2/232	122	23	145	87
1 + 2/284	148	49	197	87
BEK point (00:00–24:00)				
1/245	122	123	245	–
2/366	151	15	166	200
1 + 2/611	273	138	411	200

According to results in Table 2, the repeatability of versions 1 and 2 we are interested in above all others (197 h at the IAO point and 411 h at BEK) in general allows one to carry out for them a statistically provided analysis of the relationships between the quantities H_m and γ_m and the meteorological parameters in the surface layer. Only at the IAO point were cases of ground inversion (type 1) implemented relatively rarely (in total, 52 h), and conclusions for these cases can be only estimates.

RESULTS AND DISCUSSION

A short survey of meteorological situations under conditions in which measurements were carried out using the temperature–wind complexes was already presented in [19]. We briefly recall these results. Figure 2 shows plots of wind velocities V_h at the IAO (17 m) and BEK (10 m) points and their integral distribution functions (IDFs) both over the whole period and only for the time when temperature inversions (of all types and forms) are present in the ABL. In spite of the sig-

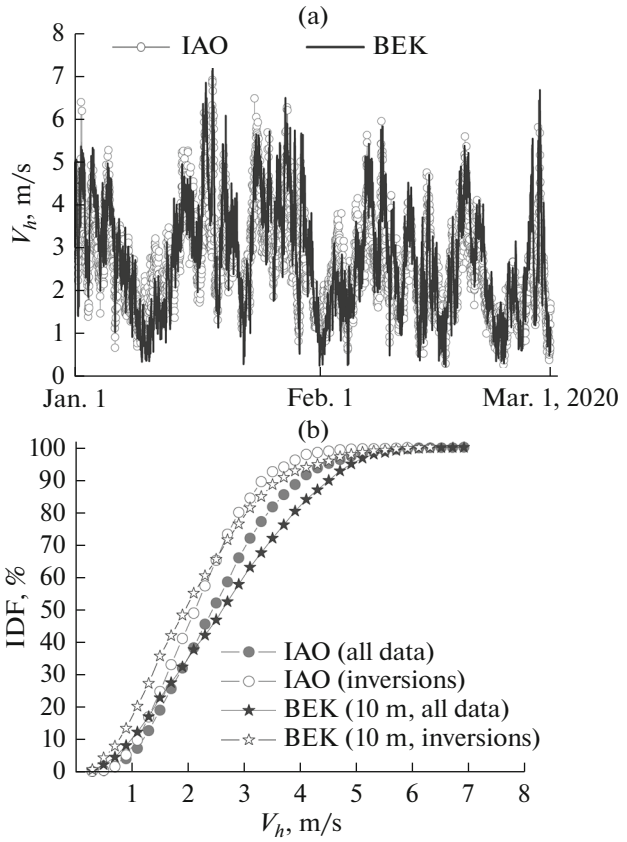

Fig. 2. (a) Wind velocity at the IAO and BEK points and (b) integral distribution functions of the wind velocity under different conditions.

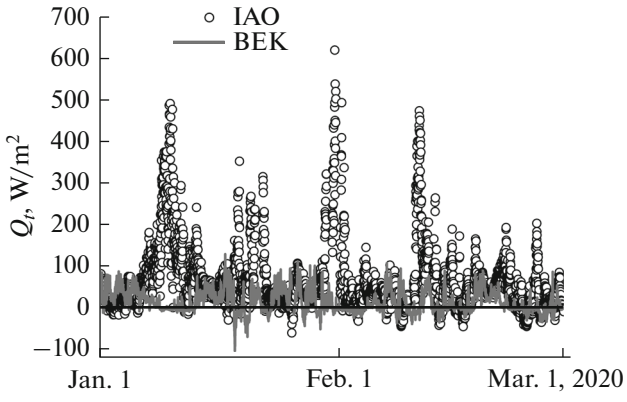

Fig. 3. Vertical turbulent heat flow at two observation points.

nificant difference in the structure of the underlying surface and distance between the points (more than 3 km), the statistics of the wind velocity at both points is approximately similar (the wind velocity at BEK was sometimes higher than at IAO).

Let us briefly present estimation results for vertical turbulent heat flows Q_t calculated by measurements

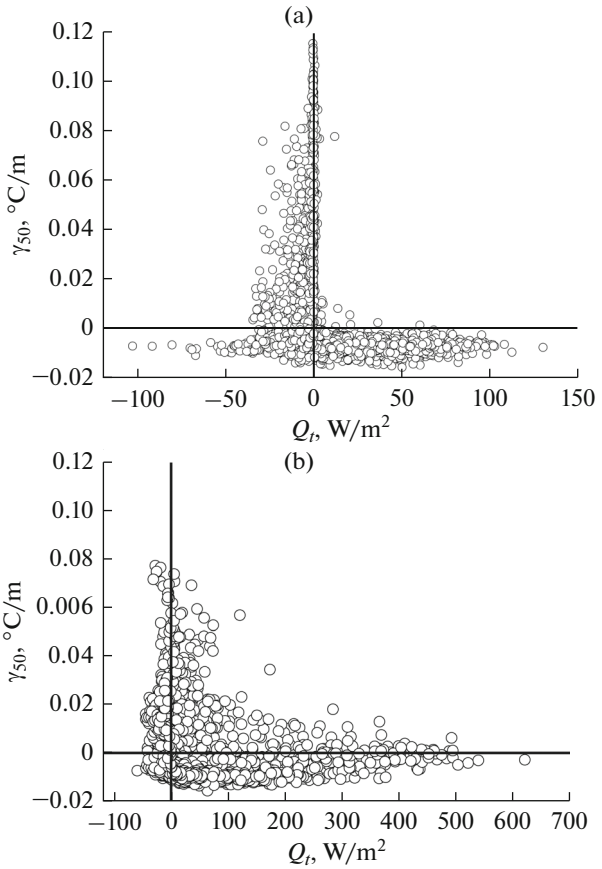

Fig. 4. Interrelation between the temperature gradient in the surface layer and vertical turbulent heat flow at the (a) BEK and (b) IAO points.

using ultrasonic meteorological stations. We recall that the IAO point is classified as urban where man-made heat sources play an active role in the formation of Q_t. Figure 3 shows plots of Q_t at the IAO and BEK points for the whole period, without selection of episodes with the presence of temperature inversions in the ABL. The technique of estimating Q_t was described, e.g., in [24]. Let us pay attention to the fact that the diurnal variations in Q_t are not so pronounced as usually in the warm period of the year.

The significant difference between the behavior of ground values of Q_t at the compared points, which should also lead to a difference between temperature profiles in the lower part of the ABL (in particular, to the dependence of temperature gradients on the magnitude of the heat flow), is evident. This conclusion is illustrated by Fig. 4 which shows the relationship between the ground gradient $\gamma_{50} = [T(50) - T(0)]/50$ (normalized difference of temperatures between levels 0 and 50 m) and the quantity Q_t.

According to the results presented in Fig. 4, the cases where the ground temperature inversion ($\gamma_{50} > 0$) was observed in the lower layer of the atmosphere at $Q_t > 0$ ($\gamma_{50} > 0$) were almost absent at the BEK point.

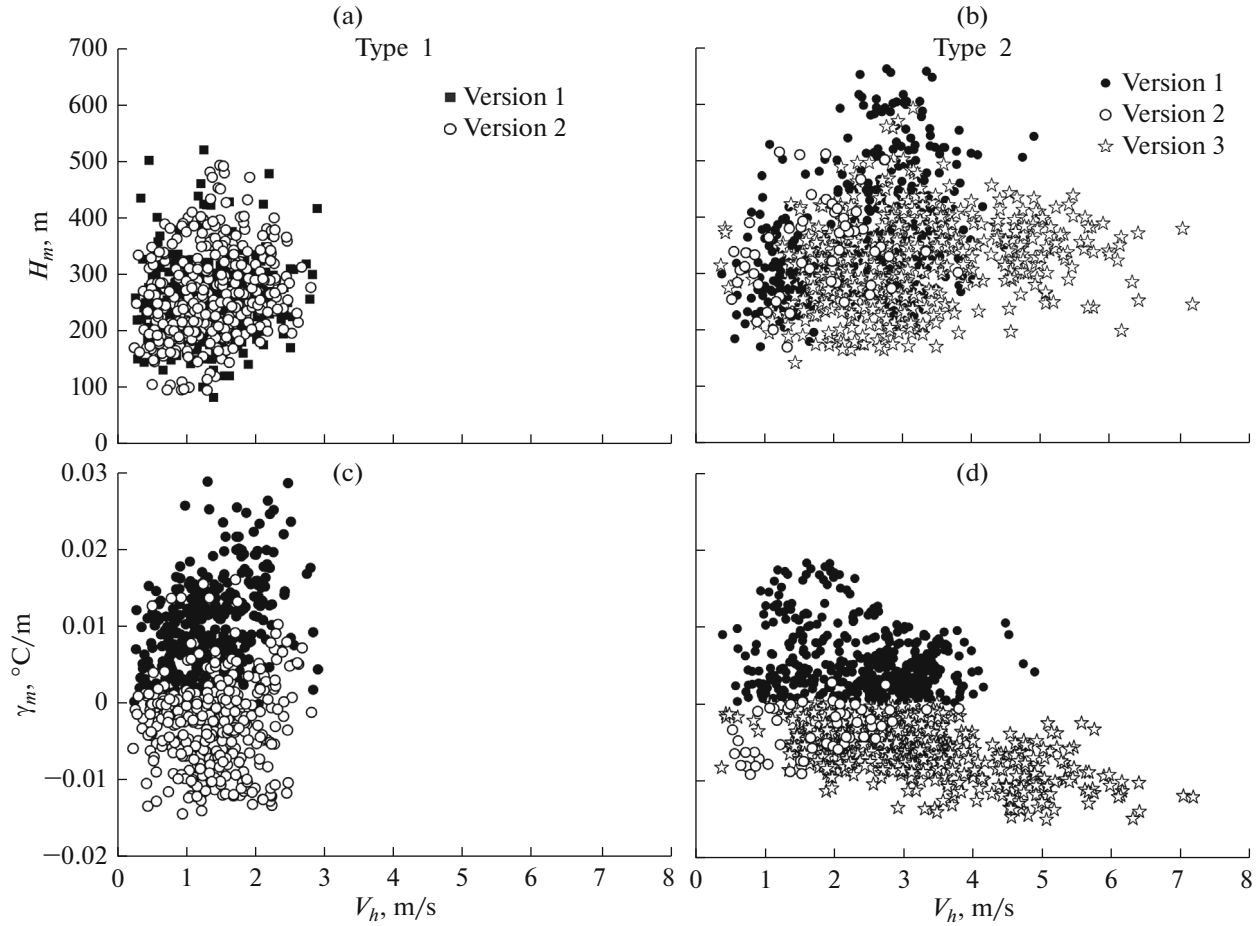

Fig. 5. Dependence of (a, b) H_m and (c, d) γ_m on V_h in the surface layer for (a, c) ground and (b, d) raised inversions of air temperature at the BEK point.

At the IAO point, on the contrary, there were many cases in which considerable positive flows Q_t generated by man-made heat sources were present under conditions of ground inversion ($\gamma_{50} > 0$). However, those sources created only *local* flows. In general, the vertical turbulent heat flow averaged over a certain area and determining the temperature in the layer 0–50 m was probably much weaker and could not destroy the existing ground temperature inversions; it only decreased temperature gradients in this layer. At the same time, a kind of the urban heat island occurred, as follows from Fig. 6 in [19] where the temperature differences between IAO and BEK in the period under study were presented.

Let us turn directly to the survey devoted to results of the analysis of how the heights H_m and temperature gradients γ_m corresponding to them are related to wind velocities V_h and turbulent heat flows Q_t in the surface layer. The general idea about the relationship $H_m(V_h)$ for different inversion types and their versions at the BEK point is shown in Figs. 5a and 5b. The plots are constructed on a common scale for better visual perception. According to the results, ground inversions (type 1, Fig. 5a) occurred only with $V_h \le 3$ m/s. In turn, raised inversions (type 2, Fig. 5b) could exist at almost any values of V_h in the observation period. However, the turbulent heat exchange could penetrate into the inversion layer only at wind velocities less than 4 m/s (with few exceptions). In general, one can conclude that, in spite of the perceptible trend of an increase in H_m with the wind velocity V_h, there is no well-formed parameterizable dependence $H_m(V_h)$. A similar conclusion is also valid for the IAO point (we leave this conclusion unillustrated).

Let us now consider results related to the dependences $\gamma_m(V_h)$ (Figs. 5c and 5d). We recall once more that full overlapping of the inversion layer by the turbulent heat exchange very often took place in the case of ground inversion (type 1, version 2, Fig. 5c). This is in reference to temperature profiles in forms 2–4 according to Fig. 1a. At the same time, the turbulent heat exchange could also penetrate into the second inversion layer (forms 3 and 4), especially when the temperature profile has form 4 (see Table 1). Similar regularities were also observed at the IAO point where, however, the statistical provision of such conclusions is poor (in

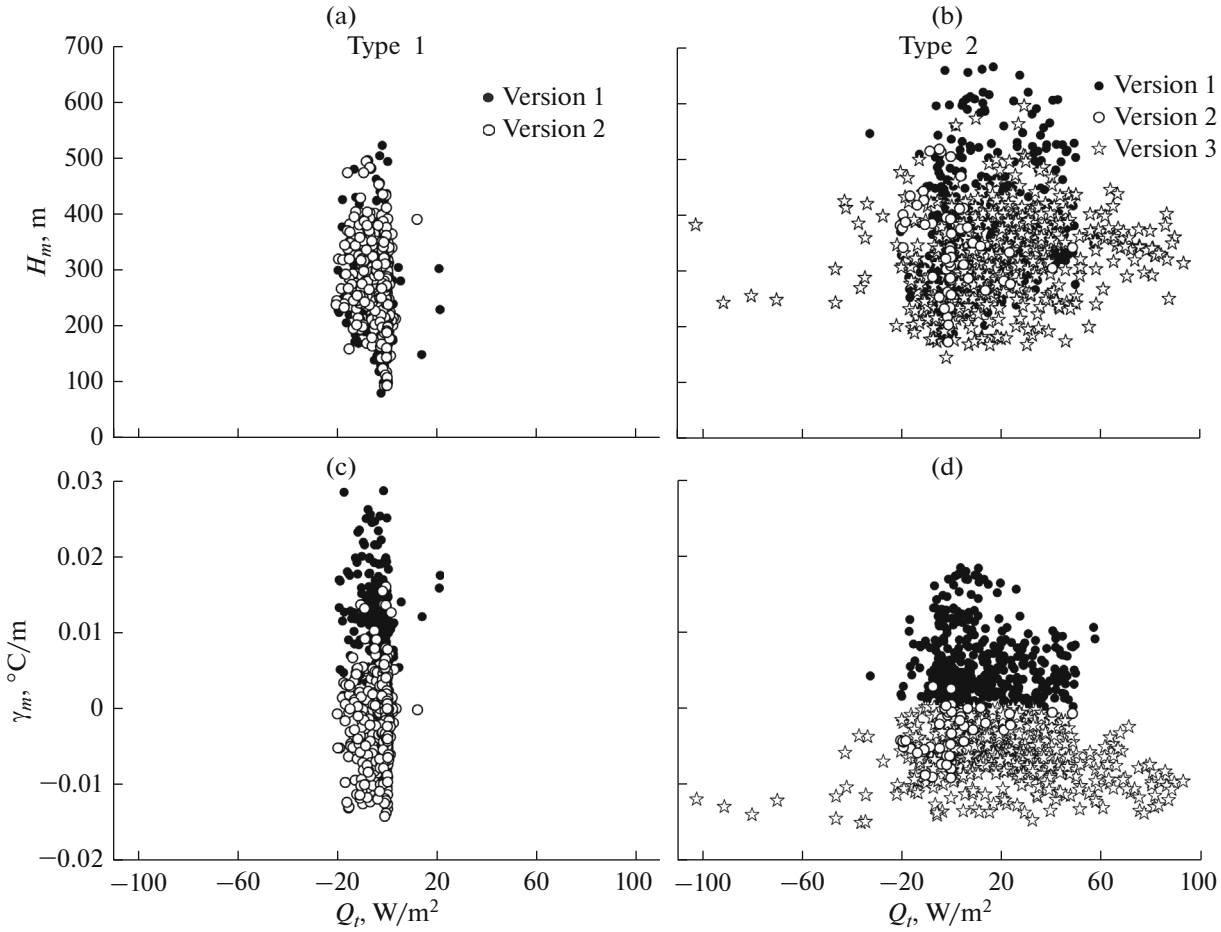

Fig. 6. Dependence of (a, b) H_m and (c, d) γ_m on Q_t in the surface layer for (a, c) ground and (b, d) raised inversions of air temperature at the BEK point.

total, 52 h of observations). We treat the result as one of the main ones in our work because it is usually assumed that the turbulent heat exchange exists only under the inversion layer (as version 3 in Fig. 5d) or does not penetrate very deep into it. It is natural that the turbulent heat exchange must destroy the ground inversion layer (or decrease temperature gradients in it). A special question of how long the ground inversion can exist under full overlapping of the abovementioned layer by the turbulent heat exchange is not considered in this work.

In the case of raised inversions (type 2, Fig. 5d), the repeatability of the inversion overlapping by the turbulent heat exchange is significantly less. In general, the dependence of γ_m on V_h is feebly marked with the exception of version 3 in Fig. 5d (the turbulent heat exchange is only under the raised inversion layer). However, a comprehensive analysis of this version was beyond the scope of our tasks. One can also mention a trend toward an increase in absolute values of γ_m in the velocity range ~1–3 m/s. This means that the turbulent heat exchange could penetrate into the inversion with steeper gradients of the air temperature.

Summarizing the analysis of interrelations of H_m and γ_m with the wind velocity V_h in the surface air layer, we emphasize that these interrelations are feebly marked at both points and the possibility of their satisfactory parameterization is almost absent. One can suppose that H_m and γ_m are stronger affected by the wind velocity (or its profile) in the whole ABL, but not only in its surface layer. We plan to turn to a comprehensive solution of this problem in further works. Preliminary results have been obtained for the IAO point and [25].

Let us now consider the interrelation of H_m and γ_m with the surface vertical turbulent heat flow Q_t. Here, we also use mainly the results obtained at BEK (owing to the good statistical provision of the estimates and continued operation of the temperature–wind complex). We immediately note that ground inversions of temperature at this point (type 1) were present only in the case of negative or vanishing values of Q_t (with the exception of few episodes). In that cases, H_m was essentially independent of the flow magnitude; it varied within the limits of (approximately) 100–500 m.

Elevated inversions (type 2) took place at all observed values of the flow Q_t. Its increase (in the positive region) favored an increase in values of H_m. However, a clearly pronounced relationship $H_m(Q_t)$ was absent. These conclusions are illustrated by Figs. 6a and 6b. They are presented on a common scale for convenience of comparison.

The interrelation between γ_m with Q_t at the BEK point was almost absent. One can only note that raised inversions (type 2) took place mainly at positive values of Q_t, and values taken by the parameter γ_m inside inversions were as small as Q_t was large (version 2 for type 2); it tended to a limit at $\gamma_m \approx 0.01$(°C/m). These conclusions are illustrated by Figs. 6c and 6d. Let us pay attention to the fact that at large (in absolute values) Q_t only raised inversions of version 3 were observed (the heat exchange occurred only under the inversion layer). Hence, the same conclusion follows as for the interrelation $H_m(Q_t)$: the possibility of a simple parameterization of the function $\gamma_m(Q_t)$ at BEK is absent.

Since the heat flows at BEK and IAO are significantly different, such conclusions for the IAO point are illustrated by Fig. 7, which presents only results corresponding to raised inversions (type 2) because the statistics are insufficient for reliable conclusions on ground inversions (type 1).

Since one-dimensional interrelations of $H_m(V_h)$, $H_m(Q_t)$, $\gamma_m(V_h)$, and $\gamma_m(Q_t)$ are not sufficiently pronounced, one can expect that complex interrelations $H_m(V_h, Q_t)$ and $\gamma_m(V_h, Q_t)$ are also weakly pronounced. For the BEK point, these interrelations are shown in Fig. 8 in the form of two-dimensional diagrams. The figure depicts only results that are related to versions 1 and 2 of the temperature inversion overlapping with the turbulent heat exchange. We recall that negative values of γ_m in these plots correspond to cases of full overlap of the temperature inversion with the turbulent heat exchange. When preparing the plots in Fig. 8, some readings containing outlier values of Q_t were excluded. In particular, when constructing the plots for ground inversions (type 1, Figs. 8a and 8c), values $Q_t > 3$ W/m^2 (and wind velocities corresponding to them) were removed; when constructing the plots for raised inversions (type 2, versions 1 and 2, Figs. 8b and 8d), we removed values $Q_t > 50$ W/m^2 and $Q_t < -20$ W/m^2. Since only several readings are excluded from the analysis (one can see them in Fig. 6), the general picture of complex interrelations does not change due to such exclusions and the plots take a more qualitative form.

The diagrams in Fig. 8 corroborate the conclusion that the trend toward an increase in H_m with the wind velocity in the surface layer is observed in the case of raised inversions (see Fig. 8b). At the same time, Q_t has almost no effect on H_m. Nevertheless, the plots allow one to distinguish trends in the interrelation $\gamma_m(V_h, Q_t)$:

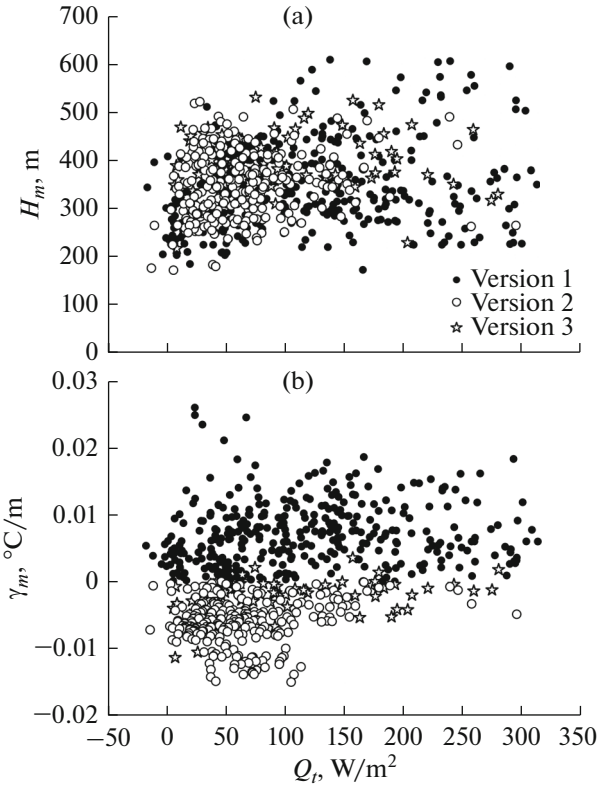

Fig. 7. Dependence of (a) H_m and (b) γ_m on Q_t in the surface layer at the IAO point in the case of raised inversions (type 2).

overlapping of temperature inversions by the turbulent heat exchange at the BEK point (region $\gamma_m \le 0$ in Figs. 8c and 8d) occurs only under certain combinations of the V_h and Q_t values and approximate fulfillment of the inequality $Q \le 0$.

Let us briefly present results for the complex interrelations $H_m(V_h, Q_t)$ and $\gamma_m(V_h, Q_t)$ at the IAO point (Fig. 9). In that case, when preparing the plots, we combined both inversion types (with the exception of version 3 from type 2). In the course of the preparation, values $Q_t > 300$ W/m^2 and $Q_t < -30$ W/m^2, as well as $V_h > 4$ m/s and $V_h < 0.9$ m/s, were excluded from the consideration.

Comparing results in Figs. 9 and 8, one can conclude that the interrelations $H_m(V_h, Q_t)$ and $\gamma_m(V_h, Q_t)$ at the BEK and IAO points are noticeably different. In addition, the possibility of a simple parameterization of these interrelations at IAO is also absent.

Summarizing the analysis of the dependence of height H_m and temperature gradients γ_m corresponding to this height on wind velocity V_h and vertical turbulent heat flow Q_t in the surface layer, we note that simple forms of this dependence do not exist. Probably, to find a possibility of predicting the H_m and γ_m values, we must include other parameters in the analysis. Ground

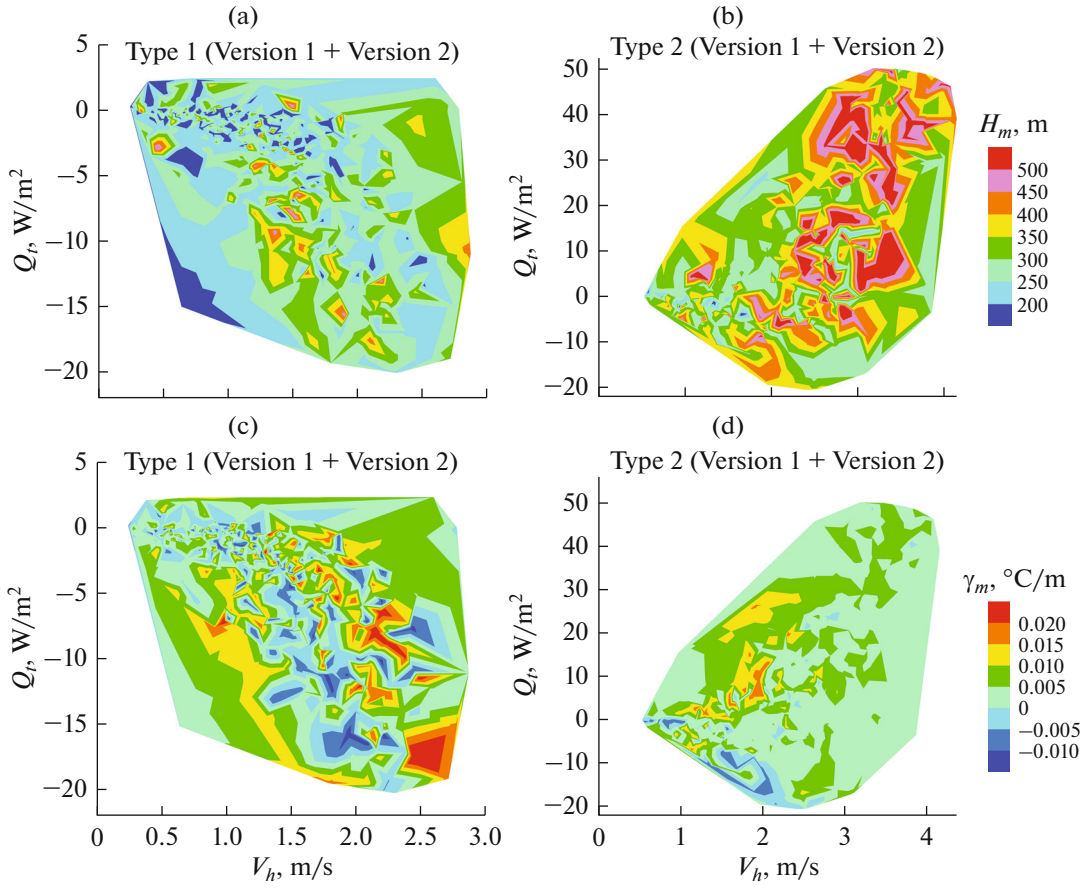

Fig. 8. Two-dimensional diagrams of the dependence of (a, b) H_m and (c, d) γ_m on V_h and Q_t for (a, c) ground and (b, d) raised elevated inversions of air temperature at the BEK point (at an altitude of 10 m).

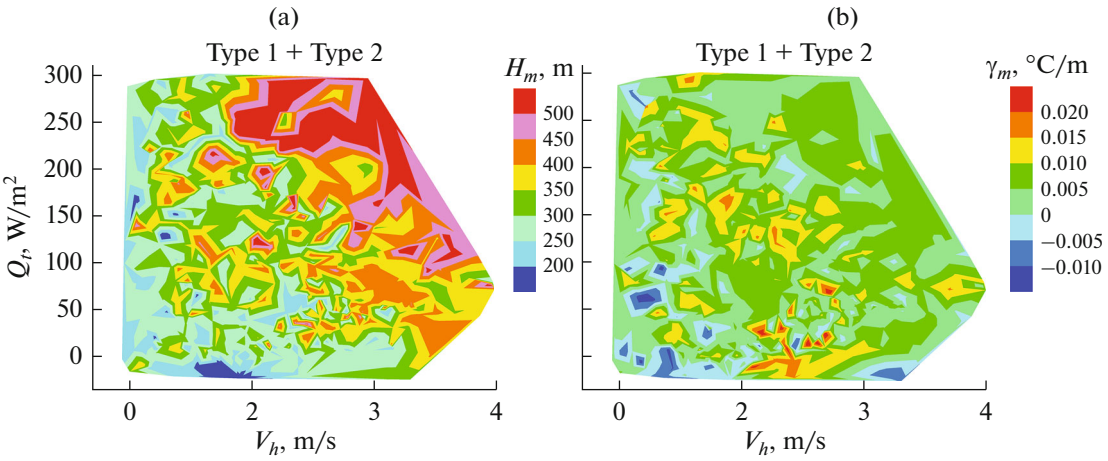

Fig. 9. Two-dimensional diagrams of the dependence of (a) H_m and (b) γ_m on V_h and Q_t at the IAO point.

values of meteorological parameters are insufficient for solving this problem under the considered conditions. In general, our conclusions coincide with those drawn from operational results from a similar temperature–wind complex in the Antarctic [9].

The involvement of data about the structure of wind and temperature fields in the ABL can significantly improve the prediction for H_m and γ_m. An example is presented by Figs. 10a, 10c, and 10d which show the dependence of γ_m on the sum of air temperature

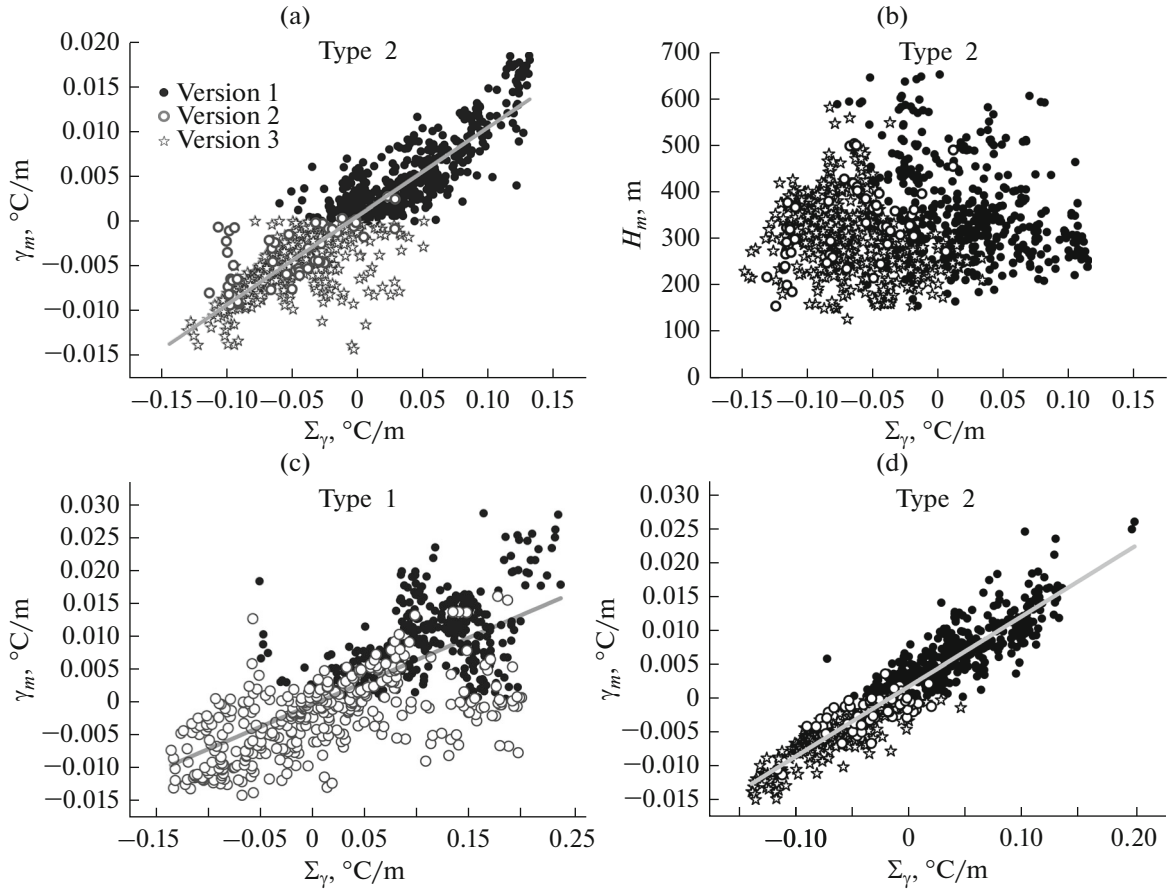

Fig. 10. Dependence of (a, c, d) γ_m and (b) H_m on the sum of temperature gradients in the layer of 0–1 km at the (a–c) BEK and (d) IAO points.

gradients over the layer 0–1 km (denoted as Σ_γ). The sum is calculated by the formula

$$\Sigma_\gamma = \frac{1}{50}\sum_{i=1}^{21}\left[T(H_i) - T(H_{i-1})\right],$$

where $T(H_i)$ is the measured (averaged over 20 min) air temperature at height H_i and the step between the heights is 50 m.

We included in Figs. 10a, 10c, and 10d all possible versions of inversions denoted by different symbols. We recall that version 2 relates to the case of full overlapping of the temperature inversion by the turbulent heat exchange and pay attention to the fact that the inversion is overlapped by the turbulent heat exchange mainly in the cases of negative values of Σ_γ. It is evident that the dependence of γ_m on Σ_γ is sufficiently well pronounced, although considerable deviations from a certain midline also occur. The midline in Fig. 10a corresponds to the result of linear approximation of the interrelation $\gamma_m^{(2B)}(\Sigma_\gamma) \approx 0.099\Sigma_\gamma$. Here and below, superscripts denote the inversion type and the point: B means BEK and I is IAO. For inversions of type 1 at BEK, a similar interrelation is also observed (Fig. 10c); the approximation has the form $\gamma_m^{(1B)}(\Sigma_\gamma) \approx 0.068\Sigma_\gamma$. For IAO and inversions of type 2, the approximation $\gamma_m^{(2I)}(\Sigma_\gamma) \approx 0.104\Sigma_\gamma$ is valid (Fig. 10d). Unfortunately, the repeatability of type 1 inversions at IAO was low (see Table 2); for this reason, we could not obtain a statistically reliable approximation for this case.

Judging from the presented examples, parameter Σ_γ is sufficiently effective for predicting γ_m. However, it is ill-suited to predicting H_m. This conclusion is illustrated by Fig. 10b, which shows the dependence $H_m^{(2B)}(\Sigma_\gamma)$. It is evident that the possibility of a satisfactory parameterization of this interrelation is absent. The same conclusion (we leave it without illustrations) also follows for $H_m^{(1B)}(\Sigma_\gamma)$, $H_m^{(1I)}(\Sigma_\gamma)$, and $H_m^{(2I)}(\Sigma_\gamma)$. Apparently, under conditions of temperature inversions, the part of the predictor for the height of the intense turbulent heat exchange layer will be played by other parameters. For example, they are the difference in the temperatures between inversion boundaries, shifts of the wind velocity in inversions, or other exter-

nal parameters related to mean fields of wind and temperature in the ABL.

CONCLUSIONS

Let us briefly summarize the main conclusions. The main purpose of this work is to verify the possibility of using data on the wind velocity and vertical turbulent heat flow directly near the underlying surface for predicting the height of the intense turbulent heat exchange layer and the air temperature gradient corresponding to this height in the planetary layer of the atmosphere under conditions of temperature inversion in winter. As a result of the analysis of experimental data obtained with the temperature–wind measurement complexes at two points (a natural landscape and an urbanized territory), it has been established that any acceptable parameterizations of the dependences we are interested in cannot be proposed. Therefore, one can bring into question results of simulation of the atmospheric boundary layer under conditions of stable temperature inversions in winter based only on the information about the state of the atmosphere near the underlying surface.

Let us also pay attention to frequently occurring effects of full overlapping of temperature inversions bounded in height by the turbulent heat exchange, which is not taken into account when simulating the atmospheric boundary layer.

In our opinion, for a more adequate simulation of turbulent heat exchange processes in the boundary layer under conditions of temperature inversions, it is necessary to involve additional information characterizing, at least in a general form, the fields of temperature and wind velocity in the boundary layer. Conceivably, information obtained only in the layer of several tens of meters from the underlying surface, but not in the whole boundary layer, can turn out to be useful. We plan to implement a similar approach in our further investigations.

ACKNOWLEDGMENTS

The experimental data were obtained using the instrumentation of the "Atmosphere" Common Use Center of the Institute of Atmospheric Optics, Siberian Branch, Russian Academy of Sciences.

FUNDING

Atmosphere characteristics were measured with financial support from the Russian Science Foundation (project no. 19-71-20042). The development of methodical aspects of the performed investigations was supported by the Ministry of Science and Higher Education of the Russian Federation.

CONFLICT OF INTEREST

The authors declare that they have no conflicts of interest.

REFERENCES

1. P. Seibert, F. Beyrich, S. E. S. E. Gryning, S. Joffre, A. Rasmussen, and P. Tercier, "Review and intercomparison of operational methods for the determination of the mixing height," Atmos. Environ. **34** (7), 1001–1027 (2000).
2. M. Burlando, E. Georgieva, and C. F. Ratto, "Parameterisation of the planetary boundary layer for diagnostic wind models," Bound.-Lay. Meteorol. **125** (2), 389–397 (2007).
3. A. M. Holdsworth and A. H. Monahan, "Turbulent collapse and recover in the stable boundary layer using an idealized model of pressure-driven flow with a surface energy budget," J. Atmos. Sci. **76** (5), 1307–1327 (2019).
4. S. S. Zilitinkevich, S. A. Tyuryakov, Yu. I. Troitskaya, and E. A. Mareev, "Theoretical models of the height of the atmospheric boundary layer and turbulent entrainment at its upper boundary," Izv., Atmos. Ocean. Phys. **48** (1), 133 (2012).
5. V. P. Yushkov, M. M. Kurbatova, M. I. Varentsov, E. A. Lezina, G. A. Kurbatov, E. A. Miller, I. A. Repina, A. Yu. Artamonov, and M. A. Kallistratova, "Modeling an urban heat island during extreme frost in Moscow in January 2017," Izv., Atmos. Ocean. Phys. **55** (5), 389–406 (2019).
6. A. F. Kurbatskii and L. I. Kurbatskaya, "Investigation of a stable boundary layer using an explicit algebraic model of turbulence," Thermophys. Aeromech. **26** (3), 335–350 (2019).
7. L. I. Kurbatskaya and A. F. Kurbatskii, "Computationally efficient turbulence model for pollution propagation simulation," Opt. Atmos. Okeana **30** (6), 524–528 (2017).
8. S. Argentini, G. Mastrantonio, and F. Lena, "Case studies of the wintertime convective boundary-layer structure in the urban area of Milan, Italy," Bound.-Lay. Meteorol. **93** (2), 253–267 (1999).
9. I. Pietroni, S. Argentini, I. Petenko, and R. Sozzi, "Measurements and parametrizations of the atmospheric boundary-layer height at Dome C, Antarctica," Bound.-Lay. Meteorol. **143** (1), 189–206 (2012).
10. M. Piringer, S. Joffre, A. Baklanov, A. Cristen, M. Deserti, K. De Ridder, S. Emeis, P. Mestayer, M. Tombrou, D. Middleton, K. Baumann-Stanzer, A. Dandou, A. Karppinen, and J. Burzynski, "The surface energy balance and the mixing height in urban areas—activities and recommendations of COST-Action 715," Bound.-Lay. Meteorol. **124** (1), 3–24 (2007).
11. G. Sgouros, C. G. Helmis, and J. Degleris, "Development and application of an algorithm for the estimation of mixing height with the use of a SODAR-RASS remote sensing system," Int. J. Remote Sens. **32** (22), 7297–7313 (2011).
12. M. Kryza, A. Drzeniecka-Osiadacz, M. Werner, P. Netzel, and A. J. Dore, "Comparison of the WRF and sodar derived planetary boundary layer height," Int. J. Environ. Pollut. **58** (1-2), 3–14 (2015).
13. M. A. Lokoshchenko, "Dynamics of thermal turbulence in the lower atmosphere over moscow from sodar observations," Rus. Meteorol. Hydrol., No. 2, 27–35 (2006).

14. A. P. Kamardin, G. P. Kokhanenko, I. V. Nevzorova, and I. E. Penner, "Joint lidar and sodar investigations of the atmospheric boundary layers," Opt. Atmos. Okeana **24** (6), 534–537 (2011).

15. H. Li, Y. Yang, X. M. Hu, Z. Huang, G. Wang, B. Zhang, and T. Zhang, "Evaluation of retrieval methods of daytime convective boundary layer height based on lidar data," J. Geophys. Res.: Atmos **122** (8), 4578–4593 (2017).

16. I. M. Brooks, "Finding boundary layer top: Application of a wavelet covariance transform to lidar backscatter profiles," J. Atmos. Ocean. Tech. **20** (8), 1092–1105 (2003).

17. M. Tombrou, D. Founda, and D. Boucouvala, "Nocturnal bounary layer height prediction from surface routine meteorological data," Meteorol. Atmos. Phys. **68** (3-4), 177–186 (1998).

18. A. K. Georgoulias, D. K. Papanastasiou, D. Melas, V. Amiridis, and G. Alexandri, "Statistical analysis of boundary layer heights in a suburban environment," Meteorol. Atmos. Phys. **104** (1-2), 103–111 (2009).

19. S. L. Odintsov, V. A. Gladkikh, A. P. Kamardin, and I. V. Nevzorova, "Height of the region of intense turbulent heat exchange in a stably stratified atmospheric boundary layer: Part 1—Evaluation technique and statistics," Atmos. Ocean. Opt. **34** (1), 34–44 (2021).

20. A. P. Kamardin, V. A. Gladkikh, S. L. Odintsov, and V. A. Fedorov, "Meteorological acoustic Doppler radar (sodar) VOLNA-4M-ST," Pribory, No. 4, 37–44 (2017).

21. E. N. Kadygrov and I. N. Kuznetsova, *Methodical Recommendations on the Use of Remote Microwave Profiler Measurements of Temperature Profiles in the Atmospheric Boundary Layer: Theory and Practice* (Fizmatkniga, Dolgoprudnyi, 2015) [in Russian].

22. E. N. Kadygrov, "Microwave radiometry of atmospheric boundary layer: Method, equipment, and applications," Opt. Atmos. Okeana **22** (7), 697–704 (2009).

23. V. A. Gladkikh and A. E. Makienko, "Digital ultrasonic weather station," Pribory, No. 7, 21–25 (2009).

24. V. A. Gladkikh and S. L. Odintsov, "Turbulent heat flux in the near-ground layer of the atmosphere and its influence on the outer scale of turbulence," Rus. Phys. J. **60** (6), 1064–1070 (2017).

25. A. P. Kamardin, V. A. Gladkikh, V. P. Mamyshev, I. V. Nevzorova, S. L. Odintsov, and I. V. Trofimov, "Estimation of the height of intense turbulent heat exchange layer in the stably stratified atmospheric boundary layer," Proc. SPIE—Int. Soc. Opt. Eng. **11560**, (2020).
https://doi.org/10.1117/12.2574268

Translated by A. Nikol'skii